JOURNAL OF GEOPHYSICAL RESEARCH, VOL. 107, NO. D19, 4372, doi:10.1029/2001JD000393, 2002

El Niño and La Niña sea surface temperature anomalies: Asymmetry characteristics associated with their wind stress anomalies

In-Sik Kang and Jong-Seong Kug
School of Earth and Environmental Sciences, Seoul National University, Seoul, Korea

Received 23 January 2001; revised 23 October 2001; accepted 24 October 2001; published 4 October 2002.

[1] The asymmetric nature of El Niño and La Niña sea surface temperature (SST) anomalies is investigated by the use of National Centers for Environmental Prediction reanalysis data and various ocean and atmosphere models. It is demonstrated that the relatively weak SST anomalies during La Niña compared with those of El Niño are related to the westward shift of wind stress anomalies by 10°–15°. The asymmetric characteristics of atmospheric responses are confirmed by the general circulation model experiments with the two different SST anomalies, which have equal amplitude but are of opposite sign from each other. The experiments with an intermediate ocean model and a hybrid coupled model clearly show that the SST anomalies over the equatorial Pacific become weaker as the zonal wind stress shifts to the west. Not only the amplitude but also the oscillation timescale of the SST anomaly is shown to be sensitive to the location of wind stress anomalies. The duration of La Niña, which is rather shorter than that of El Niño, is also related to the longitudinal displacement of the wind stress anomaly. *INDEX TERMS:* 4522 Oceanography: Physical: El Niño; 4215 Oceanography: General: Climate and interannual variability (3309); 1620 Global Change: Climate dynamics (3309); 4504 Oceanography: Physical: Air/sea interactions (0312); 3339 Meteorology and Atmospheric Dynamics: Ocean/atmosphere interactions (0312, 4504); *KEYWORDS:* El Niño, La Niña, asymmetry, zonal wind stress

Citation: Kang, I.-S., and J.-S. Kug, El Niño and La Niña sea surface temperature anomalies: Asymmetry characteristics associated with their wind stress anomalies, *J. Geophys. Res.*, *107*(D19), 4372, doi:10.1029/2001JD000393, 2002.

1. Introduction

[2] The tropical Pacific SST is oscillating on interannual timescales with a positive anomaly during El Niño and a negative anomaly during La Niña [*Philander*, 1985]. A prevailing view of the cyclic phenomenon is based on linear behavior: one extreme phase being a mirror image of the other. However, a recent study [*Hoerling et al.*, 1997] indicates that there is large nonlinearity in tropical convection and extratropical circulation anomalies during El Niño and La Niña. The nonlinearity appears not only in the atmosphere but also in the sea surface temperature (SST) anomalies. The El Niño SST anomalies tend to be greater than those during La Niña.

[3] The relatively small amplitudes of SST anomalies during La Niña compared to those of El Niño have been simulated by various kinds of ocean-atmosphere coupled models, including an intermediate coupled model [*Cane and Zebiak*, 1987] and a coupled general circulation model [*Yu and Mechoso*, 2001]. In particular, the nonlinear characteristics of SST anomalies are distinctive in *Cane and Zebiak*'s [1987] model. Herein after the model is referred to as the "CZ model." It is known that in the CZ model, the small SST anomalies during La Niña are due to the parameterization of subsurface temperature, which prevents excessive cooling beyond a certain threshold of thermocline depth. However, *Dewitte and Perigaud* [1996] showed using XBT subsurface temperature data that the subsurface temperature anomalies (T_{sub}) are symmetric for deepening and shoaling of thermocline depth. *Jin and Neelin* [1993] have used a symmetric relationship for T_{sub} as a function of the thermocline anomalies. *Kang and Kug* [2000] showed that the El Niño predictability of the CZ model is much improved when the T_{sub} parameterization is altered with a symmetric relationship. Those studies mentioned above indicate that the relatively weak SST anomalies during La Niña may not be related to a nonlinear relationship between the thermocline depth and the subsurface temperature anomalies.

[4] Ocean nonlinear dynamics other than those related to the subsurface temperature can lead to the asymmetric nature of SST anomalies during El Niño and La Niña. However, a recent study by *Hoerling et al.* [1997] indicates that the asymmetric nature may predominantly originate from the nonlinearity of the tropical atmosphere. *Hoerling et al.* [1997] showed that the tropical atmospheric responses are not linear for equal and opposite SST anomalies. During El Niño, the convection anomalies appear over the central and eastern tropical Pacific, whereas the anomalies associated with La Niña are more or less confined in the west central

0148-0227/02/2001JD000393$09.00

Pacific. This nonlinear response of convection is due to the dependency of active convection on the underlying value of the sea surface temperature [e.g., *Gadgil et al.*, 1984]. In the west Pacific warm pool region, small SST deviations from its climatological value can excite large rainfall anomalies, whereas positive SST anomalies of appreciable amplitude are required to induce convection in the eastern equatorial Pacific cold tongue region. On the other hand, negative SST anomalies in the cold tongue have no further effect on regions having normally dry conditions [*Hoerling et al.*, 1997; *Desser and Wallace*, 1990]. As a result, the convection anomaly during La Niña is shifted to the west compared to that of El Niño. The different convection anomalies can lead to contrasting wind stress patterns for El Niño and La Niña.

[5] Here, we investigate how the observed differences in atmospheric convection and wind stress can lead to the observed difference in the SST anomalies for the opposite phases of El Niño/Southern Oscillation (ENSO). A recent study by *An and Wang* [2000] shows that the equatorial SST anomaly pattern is highly sensitive to a slight zonal shift of the wind stress. In particular, they demonstrated that the interdecadal change in the structure of the ENSO mode is related to the longitudinal shift of the zonal wind stress by showing that the equatorial zonal wind stress for the high frequency decade (1962–1973) with dominant oscillation periods of 2–4 years was shifted 10° westward compared to that of the low-frequency decade (1982–1992) with oscillation periods of 4–5 years. In the present study, the sensitivity of SST anomalies to the change of the wind stress anomaly pattern is applied to understand the relatively weak SST anomaly during La Niña compared to that of El Niño.

[6] Section 2 introduces the observed data and the models utilized. The models include an intermediate ocean model and an atmospheric general circulation model (GCM). In section 3, we show the observed patterns of atmospheric and oceanic anomalies associated with El Niño and La Niña. Section 4 examines the ocean responses to various idealized wind stresses located at different longitudes using an intermediate ocean model and a hybrid coupled model. In section 5, the observed characteristics of ENSO SST variations are reproduced by a sequence of coupled model experiments with the observed wind stress patterns during El Niño and La Niña. The summary and concluding remarks are given in section 6.

2. Data and Model

[7] The data utilized are monthly means of sea surface temperature, surface wind stress, outgoing longwave radiation (OLR), and sea level height over the tropical Pacific domain between 120°E–100°W and 20°S–20°N. SST is obtained from the National Centers for Environmental Prediction (NCEP), which was constructed based on the EOF of observed SST [*Reynolds*, 1988] and reconstructed after January 1981 using the optimum interpolation technique [*Reynolds and Smith*, 1994]. The wind stress is obtained from Florida State University (FSU) and OLR from the NOAA polar-orbiting operational satellites [*Gruber and Winston*, 1978]. Since the OLR is available only in the period from July 1974 to December 1999, the same data period is used for SST and wind stress. Sea level data are taken from the reanalysis data set produced by the ocean data assimilation system in NCEP [*Ji et al.*, 1995; *Behringer et al.*, 1998]. The data period of sea level data used in this study is from January 1980 to December 1999.

[8] An intermediate ocean model similar to that of *Cane and Zebiak* [1987] is used in the present study. The only difference between the present model and that of Cane and Zebiak is the parameterization of the subsurface temperature. In the CZ model, the subsurface temperature anomaly is parameterized using the hypertangent functions of thermocline depth anomaly, which are different for different signs of the thermocline depth anomaly. The CZ parameterization for a negative case results in negative SST anomalies being kept at a small value compared to those of the positive anomalies. *Battisti* [1988] showed that the CZ model produces somewhat smaller SST and wind stress anomalies in the cold event than in the warm event. *Dewitte and Perigaud* [1996], however, demonstrated using observed data that the subsurface temperature responds symmetrically to the sign of thermocline depth. In the present study, we used a similar parameterization of subsurface temperature to that of *Dewitte and Perigaud* [1996], which is the same for both negative and positive values of the thermocline depth. This is accomplished by replacing the hypertangent function for a negative case with that of a positive case. This symmetric function is important for the present study because it precludes the ocean dynamics as a possible reason for the asymmetric behavior of El Niño and La Niña. It is also noted that the SST equation of the CZ ocean model is not completely linear due to the nonlinearity included in the advection terms. However, the asymmetries of El Niño and La Niña SST anomalies produced by the advection terms are found to be negligible (not shown).

[9] An atmospheric general circulation model (GCM) is used to reproduce the observed characteristics of atmospheric responses to given SST anomalies. The GCM is a spectral model with a triangular truncation at wave number 42 and has 20 vertical levels. The model was originally developed at the University of Tokyo and modified at Seoul National University (SNU). The physical processes included are the Nakajima two-stream scheme for long wave and short wave radiation [*Nakajima and Tanaka*, 1986], the Relaxed Arakawa-Shubert scheme, shallow convection, land surface processes, gravity wave drag, planetary boundary layer processes, and others [*Kim*, 1999]. *Kim* [1999] showed that the SNU GCM simulates reasonably well the climatological mean pattern of tropical circulation statistics and their anomalies during El Niño.

3. Observed Patterns for El Niño and La Niña

[10] Figures 1a and 1b show the composite SST anomalies for the mature phases of El Niño and La Niña, respectively. The mature phase is defined here as the three consecutive months of largest amplitude of the SST anomaly averaged over 180°E–90°W and 5°S–5°N. Five El Niño and La Niña after 1974 are used for the composite, which are listed in Table 1. The NINO3 SST values (averaged over 180°E–90°W and 5°S–5°N) and the locations of maximum wind stress anomaly for each El Niño and La Niña are also shown in Table 1. As seen in Figure 1 and Table 1, the amplitudes of SST anomalies during the mature phase of El Niño are generally larger than that of La Niña. It is noted that the composites of Figure 1 are based

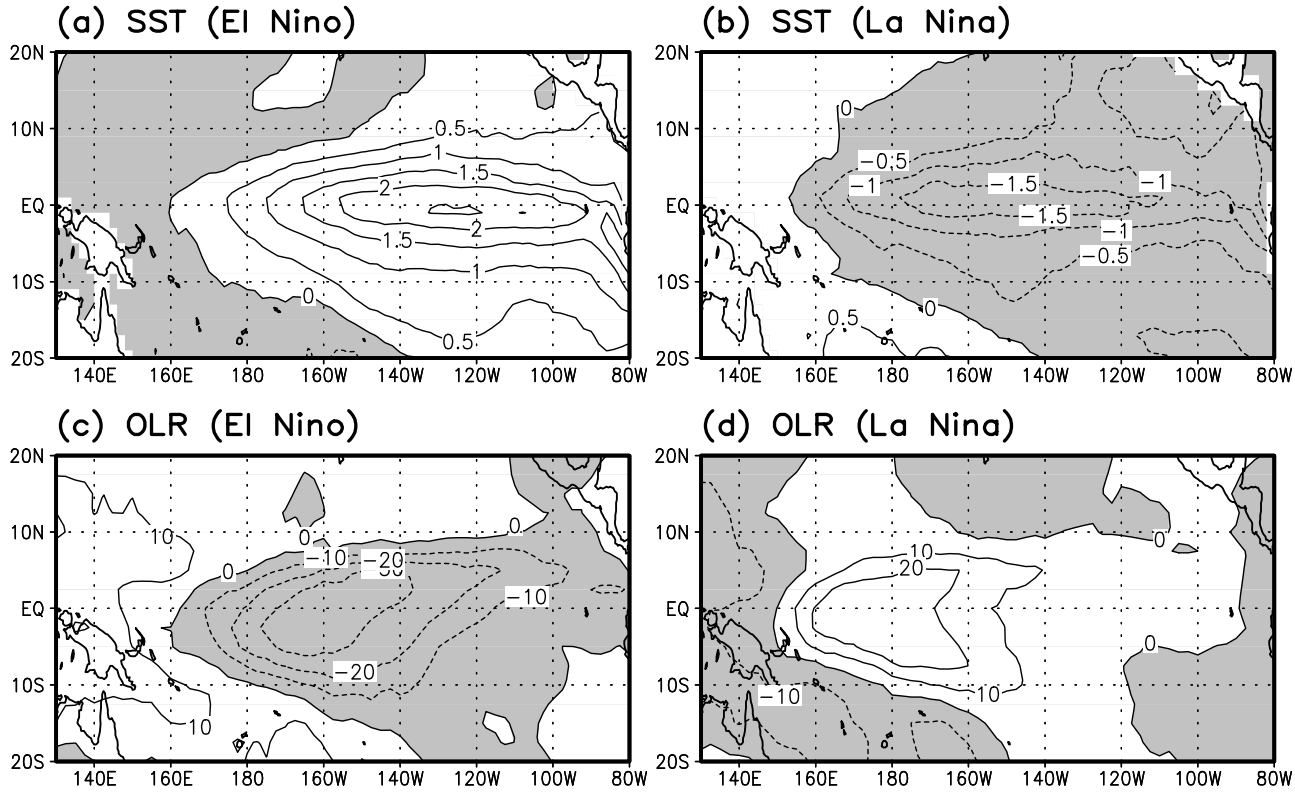

Figure 1. Composites of SST and OLR anomalies for the mature phases of El Niño and La Niña. Five El Niño and La Niña after 1974 are used for the composite. Units are °C for the SST anomalies of (a) and (b) and Wm^{-2} for the OLR anomalies of (c) and (d).

on small samples including the extremely strong El Niño for 1997–1998. However, the present results are consistent with those of *Hoerling et al.* [1997] based on a large selection of warm and cold events for 1950–1996. Their warm event composite does not include 1997–1998, and yet they too capture the asymmetry in amplitude of the SST anomalies.

[11] Figure 1 also shows that the location of the maximum SST anomaly during La Niña is shifted to the west in the central Pacific compared to that of El Niño. The spatial patterns of OLR anomalies associated with El Niño and La Niña, shown in Figures 1c and 1d, respectively, are somewhat different from each other. As pointed out by *Hoerling et al.* [1997], the difference in OLR is attributed to the zonal asymmetries of the climatological SST. In the western Pacific, the convection anomaly appears to be proportional to the SST anomaly. In the eastern Pacific, on the other hand, a strongly nonlinear relationship exists in the convective activities for different phases of the SST anomaly since a negative SST anomaly has no further effect on the relatively cold eastern Pacific [*Hoerling et al.*, 1997].

[12] It is particularly noted that the convection center during La Niña is shifted to the west compared to that of El Niño. Associated with the westward shift of OLR, the spatial pattern of zonal wind stress anomaly during La Niña shown in Figure 2b is also shifted to the west by about 15° compared to the El Niño pattern (Figure 2a). The westward shift of zonal wind and convection anomalies during La Niña can be partly related to the westward shift of the SST anomalies during La Niña (Figure 1b) compared to the El Niño SST pattern (Figure 1a). However, as discussed above, the westward shift of atmospheric responses during the negative SST phase is mainly due to the zonal asymmetry of climatological SST. It is noted that a cautionary remark may be needed for the above results due to the limited period of data used. There is a possibility of aliasing longer-

Table 1. Period Used for Composite of El Niño and La Niña[a]

El Niño			La Niña		
Period	NINO3 SST	Maximum Wind Stress	Period	NINO3 SST	Maximum Wind Stress
1997.10–97.12	3.23	163°W	1988.10–88.12	−1.66	180°E
1982.11–83.1	2.59	163°W	1975.11–76.1	−1.60	174°W
1987.8–87.10	1.37	180°E	1998.12–99.2	−1.02	174°E
1991.12–92.2	1.03	174°W	1984.12–85.2	−0.87	174°W
1976.9–76.11	0.80	158°W	1996.1–96.3	−0.72	174°E
Composite	1.81	163°W	composite	−1.09	174°E

[a]NINO3 SST and maximum wind stress indicate corresponding SST anomaly in NINO3 region and the longitude at which the maximum magnitude of wind stress averaged over 3°S–3°N occurs, respectively. Composite is that of five El Niño and La Niña.

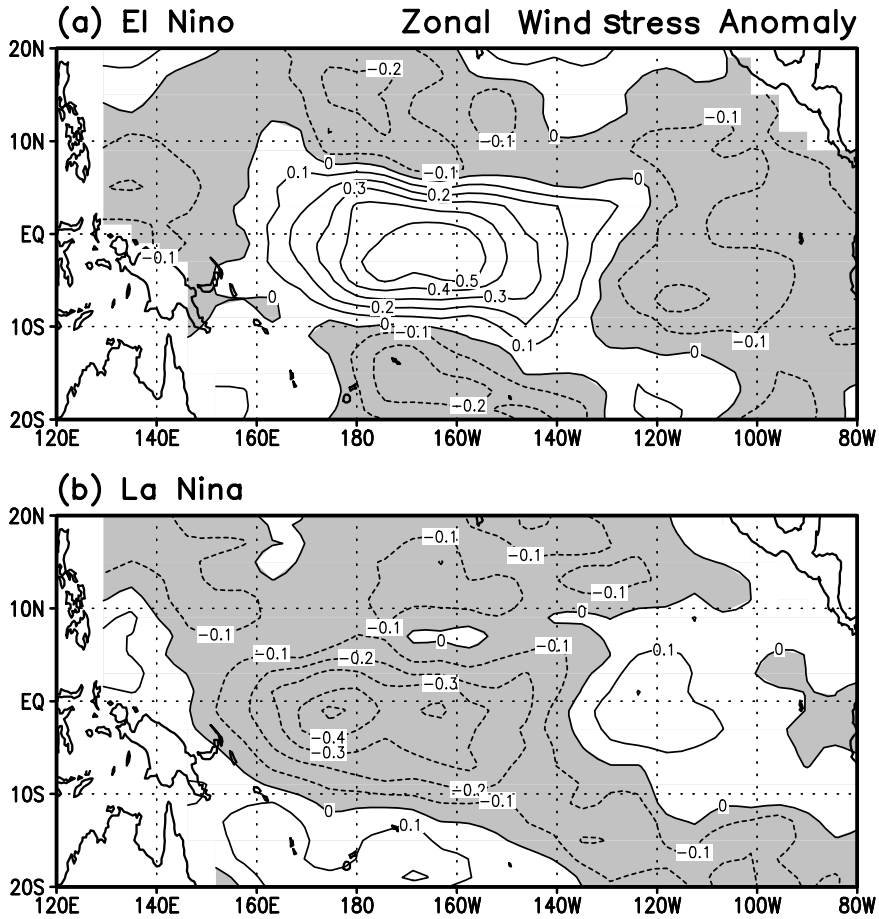

Figure 2. Composite of wind stress anomalies for the mature phases of (a) El Niño and (b) La Niña. Units are dyne cm^{-2}.

term climate variability modes in the composites. For instance, ENSO composites developed from events in the post-1974 period could well alias in the Pacific decadal oscillation. However, the asymmetric character of the SST anomalies presented above is essentially same as that obtained using the 51 year data of 1950–2000. Moreover, the GCM experiments were performed to confirm the different locations of OLR and wind anomalies during the different ENSO phases.

[13] Two sets of GCM experiments were carried out using the same pattern and amplitude of SST anomalies over the Pacific between 20°S and 20°N but with opposing signs. The objective of these experiments is to examine the nonlinear character of atmospheric responses to the different phases of SST anomalies, which is related to the zonal pattern of climatological SST. The positive and negative SST anomalies described above are obtained, respectively, by averaging the absolute values of El Niño and La Niña SST anomalies shown in Figure 1 $(SST_{El\ Niño} - SST_{La\ Niña})/2$, and by multiplying the positive anomalies by −1. In addition, one set of experiments was also performed with the climatological SST to obtain simulated anomalies of the SST anomaly runs. Each set of experiments consists of 10 ensemble runs with slightly different initial conditions. For each run, the GCM was integrated for 100 days with the Northern winter condition, and the result of each run is obtained by averaging the model output for the last 50 days. The ensemble means of surface zonal wind anomaly for the experiments with the positive and negative SST anomalies are shown in Figures 3a and 3b, respectively. The spatial pattern of the positive wind stress anomaly shown in Figure 3a is similar to that of Figure 2a and the amplitudes of both anomalies are similar when we consider the drag coefficient $C_D \sim 1.5 \times 10^{-3}$, indicating that the GCM simulates the zonal wind anomalies reasonably well. The negative wind anomaly shown in Figure 3b is not a mirror image of Figure 3a. Comparison between Figures 3a and 3b indicates that the zonal wind anomalies associated with the negative SST anomalies are a little weaker and shifted about 15° to the west compared to those of the positive SST anomalies. This result confirms the nonlinear characteristics of atmospheric responses to the SST anomalies with equal amplitude but opposing sign. It also implies that the difference between the spatial patterns of the observed wind stress anomalies during El Niño and La Niña shown in Figure 2 is mainly due to the nonlinear characteristics of atmospheric responses to the SST anomalies with different signs. In the following, we show that the zonal shift of wind stress anomalies, appearing in the different ENSO phases, results in significant changes in sea level and SST anomalies.

[14] The sea level anomalies associated with the wind stress anomalies during the mature phases of El Niño and La

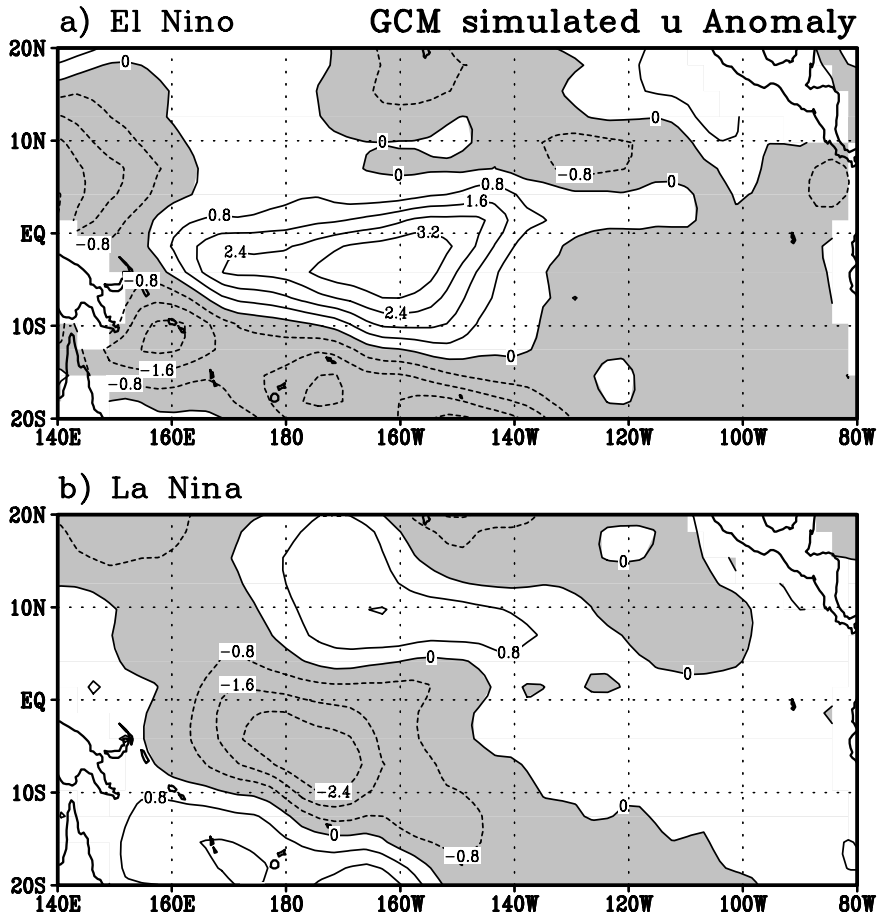

Figure 3. Distribution of the wind anomalies simulated by a GCM. (a) The difference between the 10 ensemble mean of the experiments of climatological winter-mean SST and that of the experiments with the El Niño SST anomaly shown in Figure 1a. (b) As in (a) except for the negative SST anomaly obtained by multiplying the El Niño SST anomaly by -1. Contour interval is 0.8 ms^{-1}.

Niña are shown in Figures 4a and 4b, respectively. It is clearly seen in the two figures that the amplitudes during La Niña are smaller (by about one third) than those of El Niño, particularly in the eastern tropical Pacific. The ratio between the two sea level anomalies is similar to the corresponding ratio between the SST anomalies shown in Figures 1a and 1b. This indicates that the asymmetric nature of El Niño and La Niña SST anomalies is related to the sea level anomalies, forced by different atmospheric conditions. The sea level anomaly is closely related to the thermocline depth anomaly, which directly affects SST through the mean upwelling particularly in the eastern equatorial Pacific [*Hirst*, 1988; *Kang and An*, 1998]. It is also noted that the longitude of the zero sea level anomaly coincides with that of the maximum zonal wind stress. This relationship is due to the Sverdrup balance between the wind stress and sea level height [*Jin*, 1997].

4. Oceanic Responses to Different Idealized Wind Stress Forcings

[15] In the present section, we investigate how the zonal shift of zonal wind stress results in the differences in the responses of thermocline depth and SST along the equatorial Pacific. For this purpose, the intermediate ocean model described in section 2 is forced by an idealized form of wind stress. The formula for the idealized wind stress is expressed as

$$\tau(x,y,t) = \alpha F(x,y)T(t),$$

$$F(x,y) = \{\Psi_0(y/L_y) - \Psi_2(y/L_y)\} \times \left\{ \exp\left[-\left(\frac{X - X_0}{L_x} \right)^2 \right] - 0.2 \right\}; \quad (1)$$

α is a scaling coefficient, 0.4. $F(x, y)$ is the spatial function of the wind stress adapted from *An and Wang* [2000]. ψ_0 and ψ_2 are the zeroth and the second-order Hermit functions, respectively; X_0 specifies the longitudinal position of the maximum wind stress; L_x = 35° and L_y = 9°. These values are selected such that the resulting wind stress resembles the spatial pattern similar to the observed anomalies shown in Figure 2. $T(t)$ is a time-varying sinusoidal function with a timescale of 4 years, sin (t/4 yr).

[16] The three wind stress patterns are used for the different values of X_0 = 170°E, 180°E, and 170°W, and their longitudinal distributions along the equator are shown

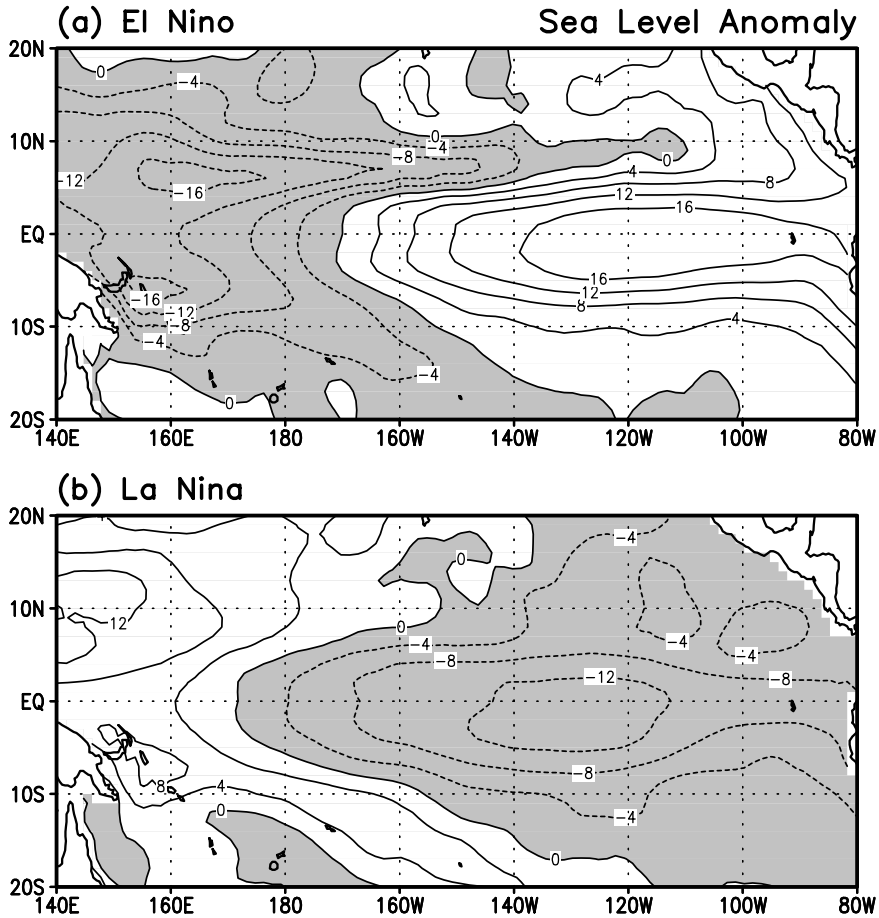

Figure 4. Composite of the sea level height anomalies for the mature phases of (a) El Niño and (b) La Niña. Contour interval is 4 cm.

in Figure 5a. The intermediate ocean model is forced by the idealized wind stresses until a regular oscillation occurred with a timescale of 4 years. Figures 5b and 5c show the thermocline depth and SST of the ocean model at the positive peak phase of SST. The figures clearly show that the location of wind stress is a crucial factor for determining both the amplitude and spatial pattern of ocean states. The node position of the thermocline depth moves according to the location of maximum wind stress, and the westward (eastward) shift of wind stress produces larger (smaller) thermocline depths in the western Pacific, whereas smaller (larger) thermocline depths are generated in the eastern Pacific. Note that the thermocline depth anomalies in the western Pacific do not affect the local SST [*Kang and An*, 1998], and therefore the large SST anomalies are confined in the eastern Pacific (Figure 5c). It is also noted that the amplitudes of SST responses doubles in the central and eastern Pacific as the center of the wind stress shifts to the east from 170°E to 170°W.

[17] Now a hybrid coupled model is used to examine the feedback between the wind stress and SST. The hybrid coupled model comprises the intermediate ocean model used above and the wind stress equation parameterized in terms of the NINO3 SST of the model. In other words, $T(t)$ in equation (1) is now replaced by the model producing NINO3 SST, and the spatial function of the wind stress used is the one in equation (1). Three different experiments have been conducted with the spatial functions $F(x,y)$ centered at 170°E, 180°E, and 170°W. As seen in Figure 6, the coupled model results are more sensitive to the wind stress position compared to those of the forced experiments shown in Figure 5 due to the positive feedback between the wind stress and SST. For the wind stress centered at 170°E, the coupled model produces a weak SST oscillation with a timescale of 2 years (Figure 6a). On the other hand, as the wind stress shifts to the east, the amplitude of oscillation becomes larger and the timescale becomes longer. The amplitude of coupled oscillation for the wind stress centered at 170°W (Figure 6c) is about 10 times greater than that of the wind stress centered at 170°E (Figure 6a). The present results clearly indicate that the ocean-atmosphere coupled system in the tropical Pacific is very sensitive to the location of wind stress anomalies.

5. Coupled Model Experiments With Observed Wind Stress Patterns

[18] In order to simulate the SST variations of ENSO more realistically, a statistical atmosphere model instead of the idealized form of wind stress is coupled to the same intermediate ocean model. The statistical atmosphere model is developed based on the singular value decomposition

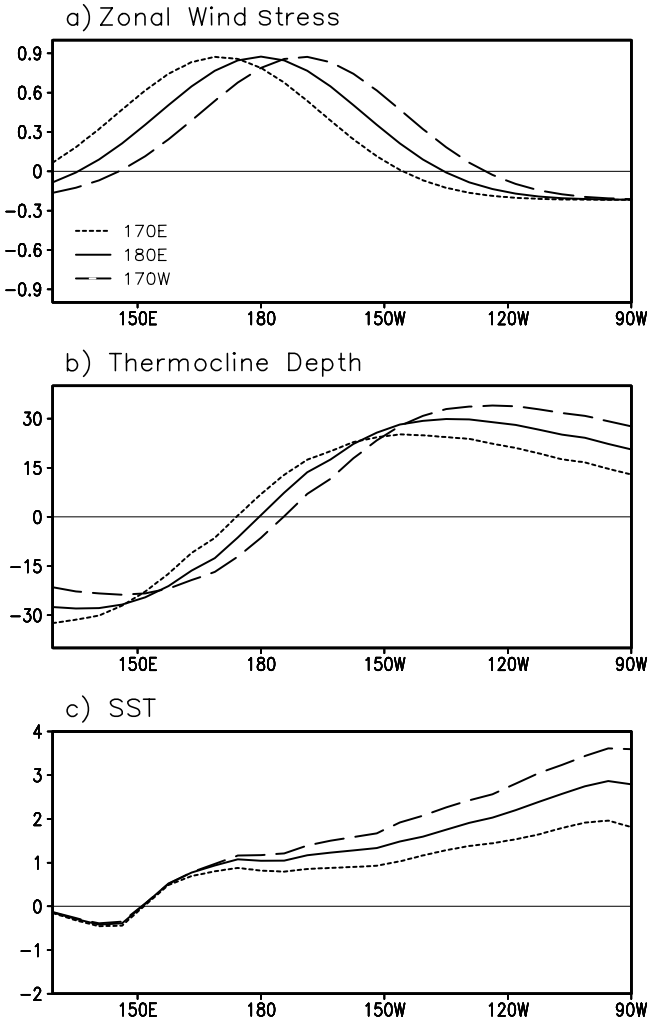

Figure 5. Responses of the intermediate ocean model to the three different wind stresses centered at 170°E, 180°E, and 170°W. Shown in (a) are the three wind stress patterns along the equator, in (b) and (c) are the thermocline depth and SST anomalies of the model along the equator.

(SVD) of observed zonal wind stress and SST [*Kang and Kug*, 2000], which can be expressed as

$$\tau(x,y) = \mu\left(\sum_x \sum_y V_{\mathrm{SST}}(x,y)\mathrm{SST}(x,y)\right) V_\tau(x,y),$$

$$\mu = \left(\sum_t T_{\mathrm{SST}}(t)T_\tau(t)\right) \Big/ \sum_t T_{\mathrm{SST}}(t)^2, \qquad (2)$$

where V_{SST} and V_τ are the SVD singular vectors for observed SST and wind stress anomalies, respectively, and T_{SST} and T_τ are the associated time series. SST is the sea surface temperature of the coupled model. The details of the present coupled model are given by *Kang and Kug* [2000]. Whereas the model of *Kang and Kug* [2000] employs two leading SVD modes, the present model makes use of the first leading mode only. The first mode of V_τ is very similar to the average of the wind stress patterns for El Niño and La Niña (Figure 2a−Figure 2b)/2. Thus the present model uses the same spatial pattern of wind stress for the positive and negative phases of NINO3 SST. The model is integrated for 50 years and the simulated ENSO-like oscillation is nearly regular after 4−5 years integration from random initial conditions. Figure 7a shows the SST variations along the equator for the 31st−40th model years produced by the coupled model. As seen in the figure, the coupled model produces an ENSO-like oscillation with a timescale of 4 years, and the SST variations show similar amplitudes for both El Niño and La Niña.

[19] The next experiment considered the effect of different wind stress patterns. For this purpose, we employed the same model used above except that the singular vector of wind stress is replaced by the observed wind stress patterns

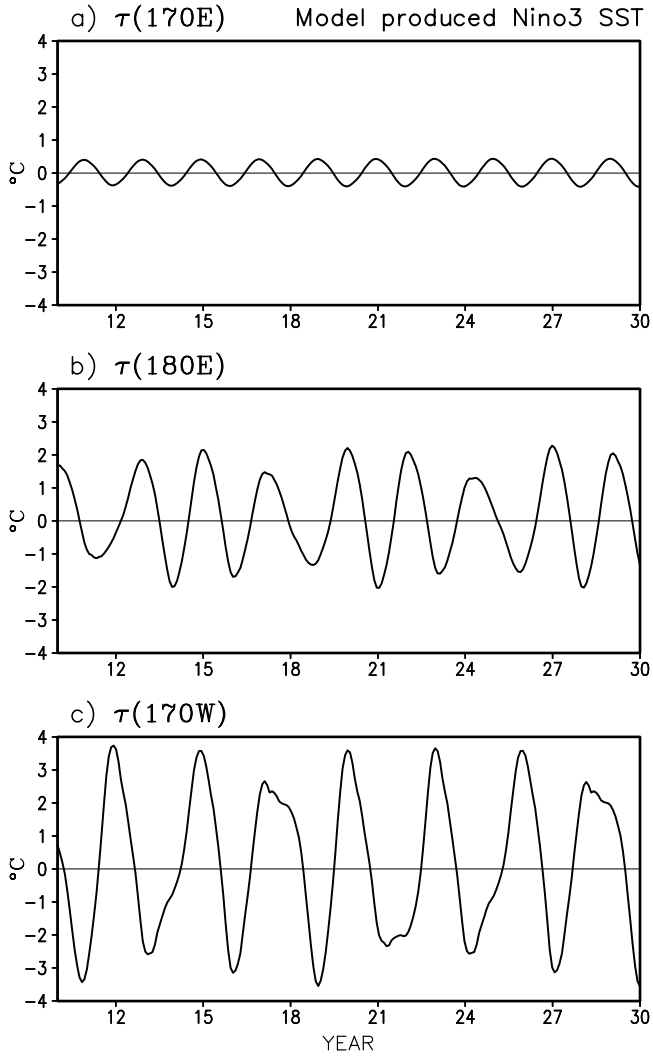

Figure 6. Time series of NINO3 SST anomalies obtained by a hybrid coupled model. The spatial functions of the wind stress used are the same as those in Figure 4, but the time variation of the wind stress is a function of NINO3 SST anomaly. (a), (b), and (c) are for the wind stress patterns centered at 170°E, 180°E, and 170°W, respectively. Units are °C.

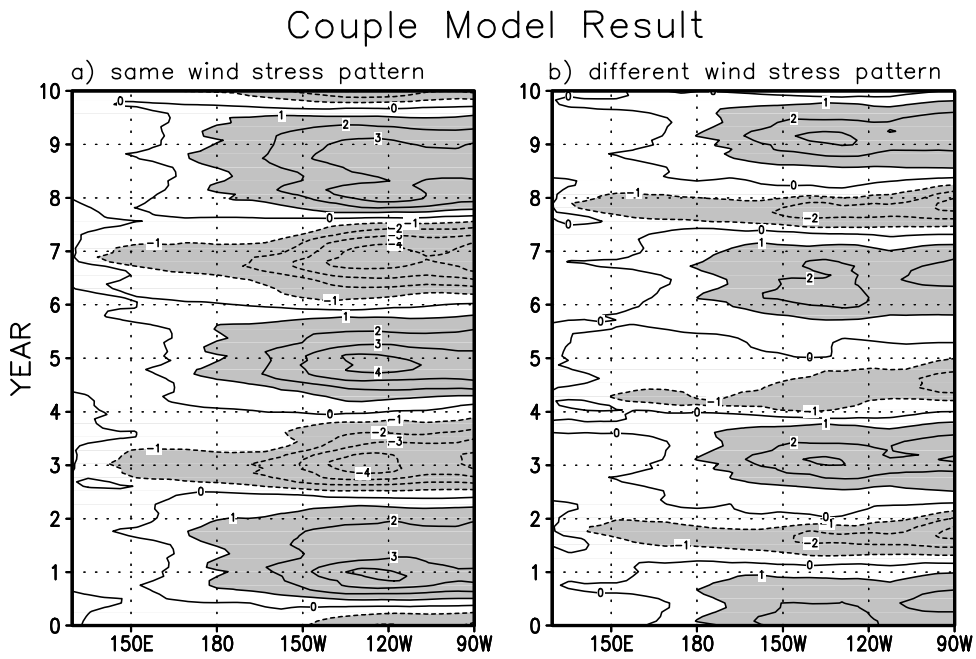

Figure 7. Variations of SST anomalies along the equator obtained using the hybrid coupled model. The wind stress is formulated using (a) the singular SVD vector of observed wind stress, and (b) the observed El Niño and La Niña composites shown in Figure 2 for the positive and negative phases of NINO3 SST. Units are °C.

of El Niño and La Niña shown in Figure 2 for the positive and negative phases of NINO3 SST, respectively. Therefore, in the present experiment, the wind stress pattern depends on the sign of NINO3 SST, even for nascent phases, but the strength of wind stress is proportional to the magnitude of NINO3 SST. In order to use the observed wind stress anomalies only in the tropical domain, the spatial function of the wind stress is multiplied by a weighting function, which is unity between 10°S and 10°N and an exponentially decaying function poleward with a zero value at 15°S and 15°N.

[20] Figure 7b shows that the duration and amplitude of El Niño SST anomaly are longer and larger, respectively, than the La Niña counterparts. This result also demonstrates that the relatively small amplitude of La Niña is due to the shift of the wind stress anomaly to the west compared to that of El Niño. Interestingly, the timescale of the oscillation is reduced to about 3 years, mainly because of the shortened duration of La Niña. It is also interesting to note that the phase change from El Niño to La Niña takes place rather quickly for about 1 year, whereas it takes about 2 years for the reversed phase change toward an El Niño. Although the experiment produces some of the observed ENSO characteristics, the oscillation is too regular and the timescale is rather short compared to the observed value.

[21] However, the model more closely simulates the observed characteristics of ENSO by adding stochastic forcing. The stochastic transient forcing is applied in a similar way to *Kirtman and Schopf* [1998], where the stochastic forcing is calculated by removing the 9-month running means from the FSU wind stress. The high-frequency transients thus obtained are randomly selected and prescribed in each time step of the coupled model integration. The coupled model used is the same as that of Figure 7b. The SST variations along the equator simulated by the model for a 20-year period are selected from a 100-year integration and shown in Figure 8a. There are certain differences in the simulations with and without the stochastic forcing. Now the variations are more irregular and the oscillation period is somewhat increased to 3–6 years, although the major characteristics such as the duration and amplitude differences between El Niño and La Niña are not much changed. These model characteristics are similar to those of the observed counterparts as shown in Figure 8b.

6. Summary and Concluding Remarks

[22] The relatively weak SST anomaly during La Niña compared to that of El Niño is demonstrated in the present study. Such a difference in the SST anomalies results from the nonlinear nature of zonal wind stress anomalies during El Niño and La Niña. In particular, the weak SST anomaly during La Niña is related to the westward shift of the wind stress anomaly by about 10°–15° compared to the wind stress during El Niño. The difference in the wind stress anomalies is associated with the different spatial distributions of convection anomalies during El Niño and La Niña. As pointed out by *Gadgil et al.* [1984] and *Hoerling et al.* [1997], the convection difference is attributed to the zonal asymmetries of the climatological SST. In the western Pacific, the convection anomaly appears to be proportional to the SST anomaly. In the eastern Pacific, on the other hand, a strongly nonlinear relationship exists in the convective activities for different phases of the SST anomaly, since negative SST anomalies have no further effect in the

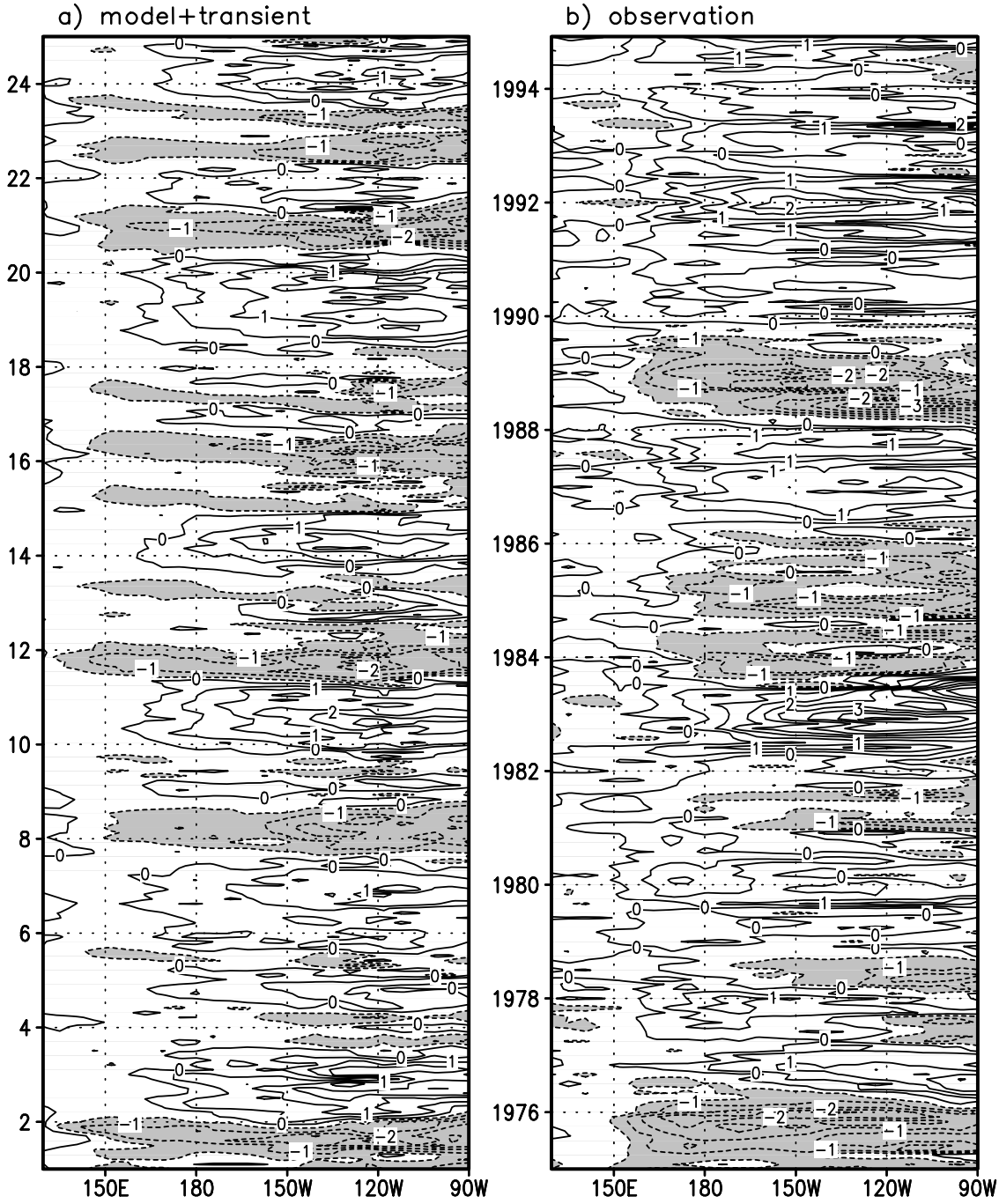

Figure 8. (a) As in Figure 7b except for the inclusion of stochastic forcing in the model. (b) as in (a) but for observations. Contour interval is 0.5°C. Negative values are shaded.

cold SST region. As a result, the convection and wind stress anomalies during La Niña are shifted to the west compared to those of El Niño. The nonlinear characteristics of the atmospheric responses for the different phases of ENSO are confirmed by the GCM experiments with two different SST anomalies of equal amplitude but opposing sign.

[23] It is pointed out that El Niño and La Niña are anomaly states with respect to a climatological basic state, but the two anomaly states of opposing sign do not have equal amplitude. Now, a critical question is raised for the oceanic and atmospheric basic states in the tropical Pacific. The basic state is usually defined as a time mean field. However, in the tropical Pacific, the climatological mean SST obtained by a long-term mean should be a little warmer than the actual SST basic state, since El Niño is larger than La Niña. Thus the time mean can be biased toward a warm condition. The present study suggests that it would be best to construct the anomalies relative to the average of "non-ENSO" years.

[24] **Acknowledgments.** This research was supported by the SRC program of the Korean Science and Engineering Foundation and the Brain Korea 21 project.

References

An, S.-I., and B. Wang, Interdecadal changes in the structure of ENSO mode and their relation to changes of ENSO frequency, *J. Clim.*, *13*, 2044–2055, 2000.

Battisti, D. S., The dynamics and thermodynamics of a warm event in a coupled atmosphere/ocean model, *J. Atmos. Sci.*, *45*, 2889–2919, 1988.

Behringer, D. W., M. Ji, and A. Leetmaa, An improved coupled model for ENSO prediction and implication for ocean initialization, part I, The ocean data assimilation system, *Mon. Weather Rev.*, *126*, 1013–1021, 1998.

Cane, M. A., and S. E. Zebiak, Prediction of El Niño events using a physical model, in *Atmosphere and Ocean Variability*, edited by H. Cattel, pp. 153–182, R. Meteorol. Soc. Press, London, 1987.

Desser, C., and J. M. Wallace, Large-scale atmosphere circulation features of warm and cold episodes in the tropical Pacific, *J. Clim.*, *3*, 1254–1281, 1990.

Dewitte, B., and C. Perigaud, El Niño-La Niña events simulated with Cane and Zebiak's model and observed with satellite and in situ data, part II, Model forced with observations, *J. Clim.*, *9*, 1188–1207, 1996.

Gadgil, S., P. V. Joseph, and N. V. Joshi, Ocean-Atmosphere coupling over monsoon regions, *Nature*, *312*, 141–143, 1984.

Gruber, A., and J. S. Winston, Earth-atmosphere radiative heating based on NOAA scanning radiometer measurements, *Bull. Am. Meteorol. Soc.*, *59*, 1570–1573, 1978.

Hirst, A. C., Slow instabilities in tropical ocean basin-global atmosphere models, *J. Atmos. Sci.*, *45*, 830–852, 1988.

Hoerling, M. P., A. Kumar, and M. Zhong, El Niño, La Niña, and the nonlinearity of their teleconnections, *J. Clim.*, *10*, 1769–1786, 1997.

Ji, M., A. Leetmaa, and J. Derber, An ocean analysis system for seasonal to interannual climate studies, *Mon. Weather Rev.*, *123*, 460–481, 1995.

Jin, F.-F., An equatorial ocean recharge paradigm for ENSO, part I, Conceptual model, *J. Atmos. Sci.*, *54*, 811–829, 1997.

Jin, F.-F., and J. D. Neelin, Modes of interannual tropical ocean-atmosphere interaction—A unified view, part I, Numerical results, *J. Atmos. Sci.*, *50*, 3477–3502, 1993.

Kang, I.-S., and S.-I. An, Kelvin and Rossby wave contributions to the SST oscillation of ENSO, *J. Clim.*, *11*, 2461–2469, 1998.

Kang, I.-S., and J.-S. Kug, An El-Nino prediction system with an intermediate ocean and a statistical atmosphere model, *Geophys. Res. Lett.*, *27*, 1167–1170, 2000.

Kim, J.-K., Parameterization of land surface processes in an atmospheric general circulation model, Ph.D. thesis, Seoul Natl. Univ., Seoul, South Korea, 1999.

Kirtman, B. P., and P. S. Schopf, Decadal variability in ENSO predictability and prediction, *J. Clim.*, *11*, 2804–2822, 1998.

Nakajima, T., and M. Tanaka, Matrix formulation for the transfer of solar radiation in a plane-parallel scattering atmosphere, *J. Quant. Spectrosc. Radiat. Transfer*, *35*, 13–21, 1986.

Philander, S. G. H., El Niño and La Niña, *J. Atmos. Sci.*, *42*, 2652–2662, 1985.

Reynolds, R. W., A real-time global sea surface temperature analysis using optimum interpolation, *J. Clim.*, *7*, 929–948, 1988.

Reynolds, R. W., and T. M. Smith, Improved global sea surface temperature analysis using optimum interpolation, *J. Clim.*, *8*, 929–948, 1994.

Yu, J.-Y., and C. R. Mechoso, Coupled atmosphere–ocean GCM study of the ENSO cycle, *J. Clim.*, *14*, 2329–2350, 2001.

I.-S. Kang and J.-S. Kug, School of Earth and Environmental Sciences, Seoul National University, Seoul, 151-742, Korea. (kang@climate.snu.ac.kr; jskug@climate.snu.ac.kr)